Operation optimization of the coaxial deep borehole heat exchanger coupled with ground source heat pump for building heating

Yaran Wang [a, b], Yeming Wang [a, b], Shijun You [a, b], Xuejing Zheng [a, *] Shen Wei [c]

[a] *School of Environmental Science and Engineering, Tianjin University, Tianjin 300350, PR China*

[b] *Key Laboratory of Efficient Utilization of Low and Medium Grade Energy, MOE, Tianjin University, Tianjin 300350, PR China*

[c] *The Bartlett School of Construction and Project Management, University College London(UCL), 1-19 Torrington Place, London WC1E 7HB, United Kingdom.*

** Corresponding author. Tel.: +086013512419172; fax: +8602227400832. E-mail addresses: zhengxuejing@tju.edu.cn*

Highlights

- ✓ The transient numerical model of the coaxial heat exchanger is established
- ✓ Operation optimization method for the heat pump system is developed
- ✓ The underground heat transfer model is validated using test data from literature
- ✓ The operation of the system before and after optimization is compared

Keywords

Coaxial deep borehole heat exchanger; Ground-coupled heat pump system; Operation optimization; Energy-saving operation

Abstract

Geothermal is considered to be one of the most promising renewable sources for district heating. Ground source heat pump systems coupled with the coaxial deep

borehole heat exchanger have been widely applied because of their high efficiency. However, in order to reduce the total energy consumption of the system, there are few studies on the optimization of the water flow rates in the coaxial deep borehole heat exchanger by time to meet the load change during the heating season. In this paper, an optimization method for the two flow rates which are set at two time periods respectively every day in the coaxial deep borehole heat exchanger during the operation of the ground source heat pump system is proposed. The application of the method is to determine the applicable flow rates when the temperature of the next day is predicted. Space heating of a building (located in Tianjin, China) is taken as a scenario, comparisons were carried out on system operation before and after optimization, which shows that the method has a good effect on the energy-saving operation of the system. After optimization, the total power consumption of the system is reduced, the total performance coefficient of the equipment as well as the temperature difference between the inlet and outlet of the underground heat exchanger is increased, and the trend of flow rates changes with time is the same as the indoor and outdoor temperature difference.

Nomenclature	
a	thermal diffusivity (m^2/s)
D	diameter (m)
h	convective heat transfer coefficient ($W/m^2 \cdot ℃^{-1}$)
m	mass flow (kg/s)
Nu	Nusselt number
Pr	Prandtl Number

Nomenclature	
r	distance from center of the coaxial deep borehole heat exchanger (m)
R	thermal resistance (m·K/W)
Re	Reynolds number
t	time (s)
T	temperature (°C)
v	velocity (m/s)
y	depth (m)
c_p	specific heat capacity of water (J/kg · K^{-1})
Q	heating capacity (W)
W	power consumption (W)
η	the efficiency of the water pump
λ	thermal conductivity (W/m · K^{-1})
λ_p	friction resistance coefficient
ρ	the density of water (kg/m^3)
Subscripts	
r	rock formations
b	backfilling material
f	fluid
in	inside diameter
out	outer diameter
ip	inner pipe
op	outer pipe
ac	annular cavity
iw	inner wall
ow	outer wall
sur	ground surface
bo	bottom
geo	geothermal
com	compressor

Nomenclature	
wp	water pump
ref	refrigerant
ep	evaporation section
esh	evaporator superheating region
cp	condensation region
csh	condenser de-superheating region
csc	condenser subcooling region

1. Introduction

The problem of energy shortage has become increasingly serious with the rapid economic growth of China [1]. However, buildings which use non-renewable energy resources are responsible for more than 30% of worldwide energy-related greenhouse gas emissions [2]. The Ground-Source Heat Pump (GSHP) systems which have the advantages of high efficiency have been widely used [3]. Compared with the Air-Source Heat Pump (ASHP) systems, the GSHP system has a higher coefficient of performance (COP) due to its stable underground temperature [4]. With the development of drilling technology, the utilization of the geothermal resource is no longer limited by drilling depth [5-7]. The depth of the Coaxial Deep Borehole Heat Exchanger (CDBHE) can be above 2000m, where there is a higher energy grade, other than the traditional GSHP system, in which the depth of the borehole is less than 300m. Besides, the reinjection and environmental pollution are difficult to solve for the traditional method of extracting geothermal hot water [8]. The CDBHE with a closed water cycle does not require reinjection, which only occupies a small footprint, and has higher heat

extraction power than the traditional method of extracting geothermal [9, 10], hence, it is a clean and efficient technology to utilize geothermal energy (Fig.1).

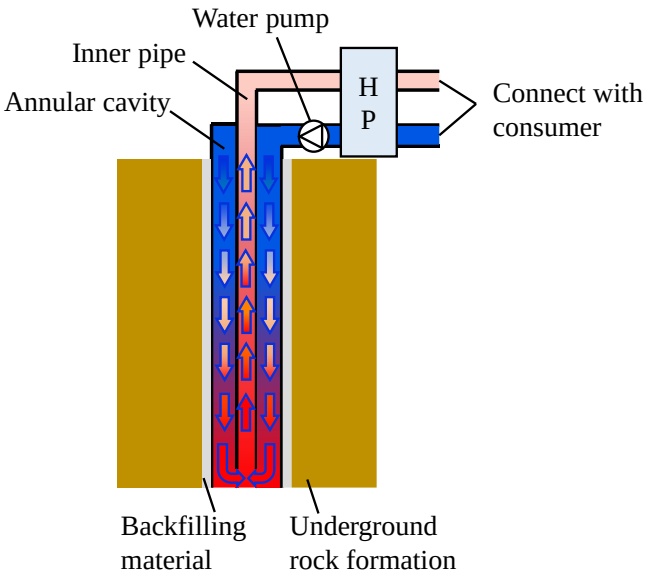

Fig. 1. Diagram of coaxial deep borehole heat exchanger

Researchers have conducted numerous studies on the heat transfer process of the CDBHE. Stefano Morchio et al. [11, 12] devoted to the analyses of Thermal Response Test (TRT) simulations aimed at understanding the main factors that influence the ground thermal conductivity and the effective borehole thermal resistance estimations. Holmberg et al. [13] developed a numerical model to study the influence of the flow direction of the mass flow and the borehole depth for the CDBHE. Peng Li et al. [14] established a three-dimensional (3D) numerical model of CDBHE for sensitivity analysis of heat transfer characteristics. Huang et al. [15] based on an open-source simulator - OpenGeoSys to discretize and solve the established three-dimensional (3D) model. To reduce the computation burden of the 3D numerical model and improve the calculation efficiency, Gordon et al. [16-18] developed a 1D radial composite cylindrical-source model for the CDBHE. They ignored the vertical fluid temperature

distribution. The unsteady-state two-dimensional (2D) numerical model is also studied. Fang et al. [19] established a 2D model considering the coupled heat transfer within the tubes and the surrounding subsurface, to analyze the influence of the borehole depth, geothermal heat flux, and thermal conductivity of the subsurface. Morchio et al. [20] developed a 2D finite-difference numerical model to analyze the effects of the pipe diameter ratio both in terms of fluid temperature evolution and pressure losses inside inner and annular pipes. Liu et al. [21] proposed a 2D numerical model which considers the comprehensive effects of the geothermal gradients and the heat loss of the inner pipe to study the influence of the inlet flow rates. Results indicate that the heat loss rate decreases as the flow rate increases, while the pumping power increases due to the higher velocity in the CDBHE. Song et al. [22] established a 2D heat transfer model to study the optimal insulation length in terms of heat insulation effect, costs, and the critical value for the flow rate to obtain higher thermal power with appropriate pressure drop. The power consumption of the water pump will decrease with the decrease of the flow, but the heat extraction power will decrease at the same time [23], which will lead to an increase in the power consumption of the heat pump under the same load on the user side.

Despite the research efforts placed on the heat transfer process of the CDBHE to extract heat as much as possible, few studies have been oriented from a total power consumption of the GSHP system perspective, whereas the lack of this perspective may lead to a biased view of system operation. Hein et al. [24] studied the relationship between flow rates and underground temperature, the relationship between flow rates

Zhang [25] studied the relationship between optimal flow rates and borehole depth for maximum heat extraction. Zhao et al. [26] optimized the flow rates and other parameters in the design stage. The total system energy consumption is not comprehensively considered in these researches [24-26]. Zarrella et al. [27] studied the relationship between the flow rate and the energy efficiency of the entire system, but under the condition of a constant temperature difference in the heat-carrier fluid across the heat pump.

The optimal value of the flow rates should be constantly optimized according to the heating load, which is related to the outdoor temperature, rather than a constant value throughout the year or other constraints [27]. At the same time, it will be closer to actual operation when considering the role of the heat pump which could provide a time-varying inlet temperature of the CDBHE. To obtain the optimal flow rate, Liu et al. [28] introduced a simple heat pump model considering the relationship between the COP of the system and the outlet temperature of the CDBHE, however, the optimization was based on a constant specific heat transfer rate. Actually, this value is constantly changing with the heat load.

In this paper, the interior-point method-based optimization technique of the flow rates in the CDBHE is proposed. Under the premise of minimizing daily system power consumption, the method could achieve that the flow rate in the CDBHE changes with the load during the heating season by iterative optimization day by day. To search for the optimal flow rates, the total power consumption of the heat pump and the circulation pump is taken as the objective function, and the hourly outdoor temperature is adopted

as the input of the model, and the constraint condition is that the heat pump output should meet the heating load demand. After optimization, the energy consumption of the system is significantly reduced.

2. Mathematical model

The mathematical model of the CDBHE heat pump system consists of three parts: the heat exchanger model, heat pump model, and pump model.

2.1 The heat exchanger model

The heat transfer process of the cylindrical area is simplified into a 2D heat transfer problem in the radial and depth directions due to the characteristics of axial symmetry, as shown in Fig.2. The flow direction of the fluid from the annular cavity to the inner pipe is employed in the proposed model, which is more conducive to extracting heat [29]. The following assumptions are considered for simplicity: (1) the underground rock formations and the backfilling material are regarded as homogeneous materials with constant physical parameters; (2) ignore the contact thermal resistance between underground rock formations and the influence of groundwater flow [23, 30], consider the pure heat conduction between the underground rock formations only; (3) the temperature gradient of the circulating fluid in the annular cavity and the inner pipe in the radial direction is neglected, only the temperature change of the circulating fluid in the depth direction is considered [28]; (4) the physical parameters of the fluid, pipes, backfilling material and underground rock formations do not change with temperature.

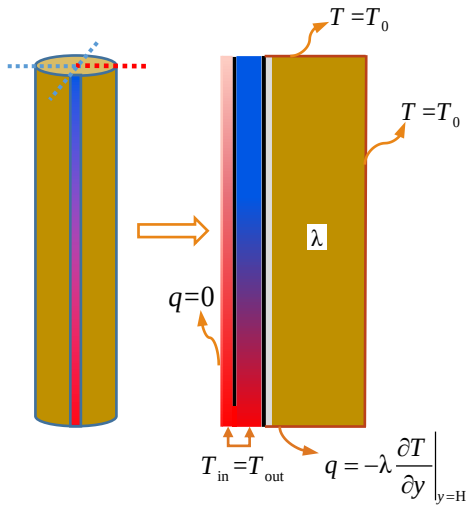

Fig. 2 Physical model

2.1.1 Governing equations

The heat transfer process involves three parts: heat exchange outside the CDBHE (heat conduction of underground rock formations and backfilling material), at the boundary of CDBHE (heat conduction on the outer pipe wall and convective heat exchange with the circulating fluid), and inside the CDBHE (convective heat transfer and heat conduction of the circulating fluid). The governing equations of underground rock formations, fluid in the inner pipe, and fluid in the annular cavity can be expressed as follow:

The energy conservation equation of the heat conduction process between underground rock formations can be written as:

$$\frac{\partial T}{\partial t}-\frac{a}{r}\frac{\partial T}{\partial r}-a\left(\frac{\partial^2 T}{\partial r^2}+\frac{\partial^2 T}{\partial y^2}\right)=0 \tag{1}$$

where T and a are temperature and thermal diffusivity of underground rock formations; t is time; r is the distance between the control volume and the center of the CDBHE; y is depth.

In terms of fluid in the CDBHE, heat transfer occurs between the inner pipe and the annular cavity and between adjacent control volumes. The energy conservation equation of the fluid in the inner pipe can be written as:

$$\frac{\partial T_{\mathrm{f,ip}}}{\partial t}-v_{\mathrm{f,ip}}\frac{\partial T_{\mathrm{f,ip}}}{\partial y}-a_{\mathrm{f,ip}}\frac{\partial^2 T_{\mathrm{f,ip}}}{\partial y^2}=S_1 \tag{2}$$

where S_1 is the rate of temperature change of the fluid in the inner pipe due to heat absorption from the fluid in the annular cavity at the same depth:

$$S_1=\frac{4\left(T_{\mathrm{f,ac}}-T_{\mathrm{f,ip}}\right)}{\pi\rho c_p D_{\mathrm{ip,in}}^2 R_{\mathrm{ip,ac}}} \tag{3}$$

where $R_{\mathrm{ip,ac}}$ is the thermal resistance between the inner pipe and the annular cavity:

$$R_{\mathrm{ip,ac}}=\frac{1}{\pi D_{\mathrm{ip,in}} h_{\mathrm{in,iw}}}+\frac{1}{2\pi\lambda_{\mathrm{ip}}}\ln\frac{D_{\mathrm{ip,out}}}{D_{\mathrm{ip,in}}}+\frac{1}{\pi D_{\mathrm{ip,out}} h_{\mathrm{in,ow}}} \tag{4}$$

where $T_{\mathrm{f,ip}}$ and $T_{\mathrm{f,ac}}$ are temperatures of fluid in the inner pipe and the annular cavity; $v_{\mathrm{f,ip}}$ and $a_{\mathrm{f,ip}}$ are the flow velocity and the thermal diffusivity of fluid in the inner pipe; $D_{\mathrm{ip,in}}$ and $D_{\mathrm{ip,out}}$ are the inner diameter and outer diameter of the inner pipe; λ_{ip} is the thermal conductivity of the inner pipe; $h_{\mathrm{in,iw}}$ and $h_{\mathrm{in,ow}}$ are convection heat transfer coefficients of the fluid in inner pipe and the inner wall of the inner pipe and the fluid in the annular cavity and outer wall of the inner pipe. The convection heat transfer coefficients can be calculated by Petukhov's equation [31]as follows:

$$h=\frac{\lambda_{\mathrm{f}} N_{uD}}{D_{\mathrm{h}}} \tag{5}$$

$$N_{uD}=\frac{\left(\mathrm{Re}_{D_h}-1000\right)(f/8)P_{\mathrm{r}}}{12.7(f/8)^{0.5}(P_{\mathrm{r}}^{2/3}-1)+1} \tag{6}$$

where λ_{f} is the thermal conductivity of fluid; f is Darcy friction factor, which is given as:

$$f = (0.79\ln(\mathrm{Re}_{D_h})1.64)^{-2} \tag{7}$$

where D_h is the equivalent diameter.

The energy conservation equation of the fluid in the annular cavity can be written as:

$$\frac{\partial T_{f,ac}}{\partial t} + v_{f,ac}\frac{\partial T_{f,ac}}{\partial y} - a_{f,ac}\frac{\partial^2 T_{f,ac}}{\partial y^2} = S_2 + S_3 \tag{8}$$

where S_2 and S_3 are the temperature change rates of the fluid in the annular cavity due to heat absorption from the fluid in the inner pipe and the rock formation at the same depth, respectively:

$$S_2 = \frac{4\left(T_{f,ip} - T_{f,ac}\right)}{\pi\rho c_p\left(D_{op,in}^2 - D_{ip,out}^2\right)R_{ch}} \tag{9}$$

$$S_3 = \frac{4\left(T - T_{f,ac}\right)}{\pi\rho c_p\left(D_{op,in}^2 - D_{ip,out}^2\right)R_{ac,r}} \tag{10}$$

where $R_{ac,r}$ is the thermal resistance between the fluid in the annular cavity and underground rock formations:

$$R_{ac,r} = \frac{1}{\pi D_{op,in}h_{ac,iw}} + \frac{1}{2\pi\lambda_{op}}\ln\frac{D_{op,out}}{D_{op,in}} + \frac{1}{2\pi\lambda_b}\ln\frac{D_{b,out}}{D_{b,in}} \tag{11}$$

where $v_{f,ac}$ and $a_{f,ac}$ is the flow velocity and the thermal diffusivity of the fluid in the annular cavity; $D_{op,in}$ and $D_{op,out}$ are the inner diameter and outer diameter of the outer pipe; $D_{b,in}$ and $D_{b,out}$ are the inner diameter and outer diameter of the backfilling material; $h_{ac,iw}$ is the convection heat transfer coefficient of the fluid in the annular cavity and inner wall of the outer pipe; λ_{op} and λ_b are the thermal conductivity of the outer pipe and backfilling material.

2.1.2 Initial and boundary conditions

In the initial state, the fluid is static in the pipe. The temperature of the fluid is the same as the underground temperature distribution along the depth direction. The initial temperature distribution is:

$$T(i) = T_{\text{sur}} + \left[\frac{1}{2} + (i-1)\right] dy \frac{\partial T}{\partial y}\Big|_{t=0} \tag{12}$$

where i is the layer of discrete points, $1 \le i \le M$; M is the number of layers of the control volume divided in the depth direction; T_{sur} is the ground surface temperature; dy is the distance between adjacent discrete points in the depth direction.

The boundary conditions (Fig.2) on the top and right boundaries of the underground are maintained as the initial temperature distribution (ground surface temperature of the top boundary, and constant temperature gradient of the right boundary as the depth increases). Since the earth's heat flow is considered to be uniform, the second type of boundary condition is considered for the bottom boundary, which is given as Eq. (13):

$$q_{\text{b,r}} = q_{\text{b,r}}\big|_{t=0} \tag{13}$$

The third type of boundary condition is adopted for the left boundary of the underground rocks, described by Eq. (14):

$$q_{\text{ac,r}} = \frac{T_{\text{f,ac}} - T}{R_{\text{ac,r}}} \tag{14}$$

2.1.3 Equations discretization

In this work, the energy conservation equation of fluid in the annular cavity, fluid in the inner pipe, and underground rock formations are discretized with the internal node method (Fig.3).

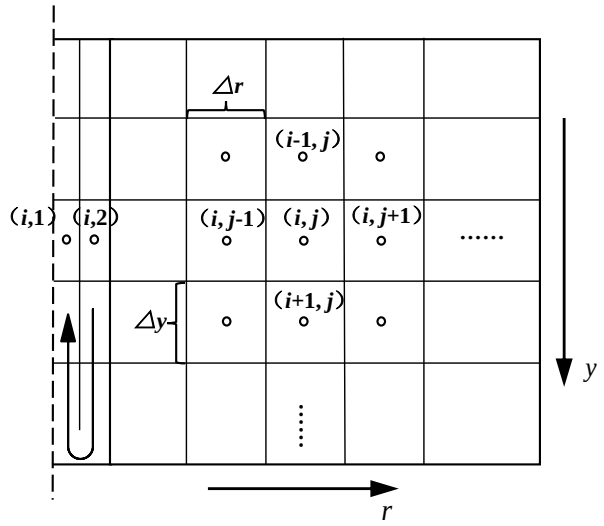

Fig. 3 Spatial discretization with inner node method

The energy conservation equation of underground rock formations is discretized by the alternating-direction-implicit (ADI) scheme proposed by Peaceman and Rachford which is absolutely stable for two-dimensional problems without time step limitation [32-35]. And the energy conservation equations of fluid and underground rock formations are discretized with different time steps.

For the discretization of the underground heat conduction equation, divide into two half time steps (from instant n-1 to n-1/2 and instant n-1/2 to n) in every two consecutive time levels (from instant n-1 to n). In the first half time step, the equation is expressed as:

$$A_{i,j-1}T_{i,j-1}^{n-\frac{1}{2}}+A_{i,j}T_{i,j}^{n-\frac{1}{2}}+A_{i,j+1}T_{i,j+1}^{n-\frac{1}{2}}-B_{i-1,j}T_{i-1,j}^{n-1}-B_{i,j}T_{i,j}^{n-1}-B_{i+1,j}T_{i+1,j}^{n-1}=0 \tag{15}$$

where

$$A_{i,j-1}=-\frac{a}{\Delta r^2}+\frac{a}{2r_j\Delta r},\ A_{i,j}=\frac{2}{\Delta t_{\mathrm{r}}}+\frac{2a}{\Delta r^2},A_{i,j+1}=-\frac{a}{\Delta r^2}-\frac{a}{2r_j\Delta r},$$

$$B_{i-1,j}=B_{i+1,j}=\frac{a}{\Delta y^2},\ B_{i,j}=\frac{2}{\Delta t_{\mathrm{r}}}-\frac{2a}{\Delta y^2}$$

where r_j is the distance from the jth to the center of the CDBHE, $1\leqslant j\leqslant N$.

The discretized equation for the underground heat conduction in the second half time step is expressed as:

$$A'_{i-1,j}T^{\,n}_{i-1,j}+A'_{i,j}T^{\,n}_{i,j}+A'_{i+1,j}T^{\,n}_{i+1,j}-B'_{i,j-1}T^{\,n-\frac{1}{2}}_{i,j-1}-B'_{i,j}T^{\,n-\frac{1}{2}}_{i,j}-B'_{i,j+1}T^{\,n-\frac{1}{2}}_{i,j+1}=0 \tag{16}$$

where

$$A'_{i-1,j}=-\frac{a}{\Delta y^2},\ A'_{i,j}=\frac{2}{\Delta t_{\mathrm{r}}}+\frac{2a}{\Delta y^2},A'_{i+1,j}=-\frac{a}{\Delta y^2},$$

$$B'_{i,j-1}=\frac{a}{\Delta r^2}-\frac{a}{2r_j\Delta r},\ B'_{i,j}=\frac{2}{\Delta t_{\mathrm{r}}}-\frac{2a}{\Delta r^2},\ B'_{i,j+1}=\frac{a}{2r_j\Delta r}+\frac{a}{\Delta r^2}$$

The discretized equation for fluid in the inner pipe is expressed as:

$$A_{\mathrm{f,ip},i-1}T^{\,n}_{\mathrm{f,ip},i-1}+A_{\mathrm{f,ip},i}T^{\,n}_{\mathrm{f,ip},i}+A_{\mathrm{f,ip},i+1}T^{\,n}_{\mathrm{f,ip},i+1}=BT^{\,n-1}_{\mathrm{f,ip},i}+A_{\mathrm{f,ip,ac}}T^{\,n-1}_{\mathrm{f,ac},i} \tag{17}$$

where

$$A_{\mathrm{f,ip},i-1}=-\frac{a_{\mathrm{f}}}{\Delta y^2},\ A_{\mathrm{f,ip},i}=\frac{1}{\Delta t_{\mathrm{f}}}+\frac{v_{\mathrm{f,ip}}}{\Delta y}+\frac{2a_{\mathrm{f}}}{\Delta y^2}+\frac{4}{\pi\rho c_p D^2_{\mathrm{ip,in}}R_{\mathrm{ip,ac}}},$$

$$A_{\mathrm{f,ip},i+1}=-\frac{v_{\mathrm{f,in}}}{\Delta y}-\frac{a_{\mathrm{f}}}{\Delta y^2},A_{\mathrm{f,ip,ac}}=\frac{4}{\pi\rho c_p D^2_{\mathrm{ip,in}}R_{\mathrm{ip,ac}}},B=\frac{1}{\Delta t_{\mathrm{f}}}$$

The discretized equation for fluid in the annular cavity is expressed as:

$$A_{\mathrm{f,ac},i-1}T^{\,n}_{\mathrm{f,ac},i-1}+A_{\mathrm{f,ac},i}T^{\,n}_{\mathrm{f,ac},i}+A_{\mathrm{f,ac},i+1}T^{\,n}_{\mathrm{f,ac},i+1}-BT^{\,n-1}_{\mathrm{f,ac},i}-A_{\mathrm{f,ac},i,1}T^{\,n-1}_{i,1}-A_{\mathrm{f,ac,ip}}T^{\,n-1}_{\mathrm{f,ip},i}=0 \tag{18}$$

where

$$A_{\mathrm{f,ac},i-1}=-\frac{a_{\mathrm{f}}}{\Delta y^2}-\frac{v_{\mathrm{f,ac}}}{\Delta y},\ A_{\mathrm{f,ac},i}=\frac{v_{\mathrm{f,ac}}}{\Delta y}+B-2A_{\mathrm{f,ac},i+1}+A_{\mathrm{f,ac,ip}}+A_{\mathrm{f,ac},i,1},$$

$$A_{\mathrm{f,ac},i+1}=-\frac{a_{\mathrm{f}}}{\Delta y^2},A_{\mathrm{f,ac,ip}}=\frac{4}{\pi\left(D^2_{\mathrm{op,in}}-D^2_{\mathrm{ip,out}}\right)\rho c_p R_{\mathrm{ip,ac}}},A_{\mathrm{f,ac},i,1}=\frac{4}{\pi\left(D^2_{\mathrm{op,in}}-D^2_{\mathrm{ip,out}}\right)\rho c_p R_{\mathrm{ac,r}}}$$

2.2 The heat pump and pump model

The constraint condition of the optimization process is that the heating capacity of

the GSHP system always meets the given heating demand. And the partial load is considered in the heat pump model. The heating capacity of the GSHP system is identical to the sum of the underground heat extraction and the power consumption of the compressor, which is given as [28]:

$$Q_{sys} = Q_{geo} + Q_{com} = Q_{load} \tag{19}$$

where Q_{load} is the given heating demand, Q_{sys} is the heating capacity of the GSHP system, Q_{geo} is the heat extraction from underground, and Q_{com} is the heat extraction due to work of the compressor.

The two main power-consuming equipment of the GSHP system, the heat pump and water pump are considered in the proposed model. The total coefficient of performance (TCOP) is employed as an index to evaluate the energy efficiency of the GSHP system, which is given as:

$$TCOP = Q_{sys} / (Q_{com} + Q_{wp}) \tag{20}$$

Where Q_{wp} is the water pump consumption.

2.2.1 The heat pump model

The evaporator, compressor, condenser, and expansion valve are the main components of the HP, of which the *P-h* diagram is shown in Fig. 4. The subscripts e1, e3, c1, and c4 co to the conditions of evaporator inlet, evaporator outlet, condenser inlet, and condenser outlet, respectively. Besides, the subscripts e3 and c1 also indicate the compressor inlet and outlet conditions.

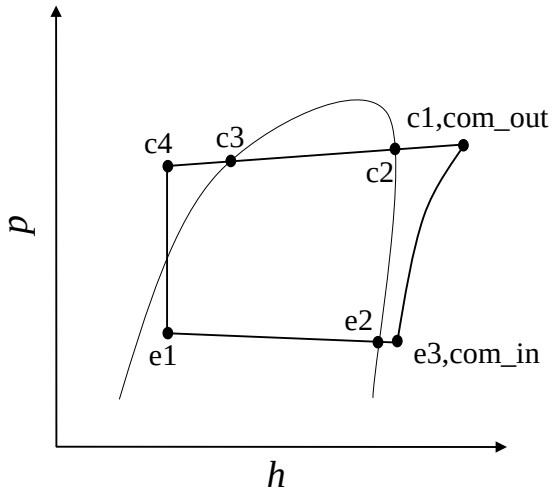

Fig. 4 The *P-h* diagram of the heat pump

The three loops (including the evaporator, the compressor, and the condenser) are modeled as follows:

The brazed-platerrespond heat exchanger is employed in evaporator and condenser sub-models. The steady-state heat exchange behavior of the evaporation is modeled by the NTU method which is given in ASHRAE Fundamentals [37]:

$$Q_{\mathrm{ep}} = m_{\mathrm{ref}}(h_{\mathrm{e}_2} - h_{\mathrm{e}_1}) = m_{\mathrm{w}}\,\mathrm{c}_{\mathrm{w}}(\mathrm{T}_{\mathrm{w,e}_2} - T_{\mathrm{w,out}}) = (1-\mathrm{e}^{-\mathrm{UA/C}})m_{\mathrm{w}}\,\mathrm{c}_{\mathrm{w}}(\mathrm{T}_{\mathrm{w,e}_2} - T_{\mathrm{e}_1}) \qquad (21)$$

where Q_{ep} is the heat transfer in the evaporation section; m_{ref} and m_{w} are the mass flow rate of the refrigerant and water; h_{e2} and h_{e1} are the enthalpies of the refrigerant in e_1 and e_2 states; c_{w} is the specific heat capacity of water;

For the evaporator superheating region, while keeping both hot and cold streams unmixed, the energy conservation equation can be expressed as [38]:

$$Q_{\mathrm{esh}} = m_{\mathrm{ref}}(h_{\mathrm{e}_3} - h_{\mathrm{e}_2}) = \mathrm{m}_{\mathrm{w}}\mathrm{c}_{\mathrm{w}}(\mathrm{T}_{\mathrm{w,in}} - T_{\mathrm{w,e}_2}) = \frac{1-\mathrm{e}^{-NTU(1-\alpha_{\mathrm{esh}})}}{1-\alpha_{\mathrm{esh}}\mathrm{e}^{-NTU(1-\alpha_{\mathrm{esh}})}} C_{\mathrm{esh\_min}}(\mathrm{T}_{\mathrm{w,in}} - T_{e_2}) \qquad (22)$$

where

$$\alpha_{\text{esh}} = \frac{C_{\text{esh\_min}}}{C_{\text{esh\_max}}} = \frac{\min(\mathrm{m_w}, \mathrm{m_w}\frac{h_{\mathrm{e_3}} - h_{\mathrm{e_2}}}{T_{\mathrm{e_3}} - T_{\mathrm{e_2}}})}{\max(\mathrm{m_w}, \mathrm{m_w}\frac{h_{\mathrm{e_3}} - h_{\mathrm{e_2}}}{T_{\mathrm{e_3}} - T_{\mathrm{e_2}}})} \tag{23}$$

Jähnig's compressor work model [39] is employed in the proposed model. The compressor motor power is given as:

$$W_{\text{com}} * \eta_{\text{com}} = m_{\text{ref}} \left(\frac{n_{\mathrm{s}}}{n_{\mathrm{s}} - 1}\right) \left(\frac{P_{\text{com,in}}}{\rho_{\text{com,in}}}\right) \left(\left(\frac{P_{\text{com,out}}}{P_{\text{com,in}}}\right)^{\frac{n_{\mathrm{s}}-1}{n_{\mathrm{s}}}} - 1\right) \tag{24}$$

where

$$n_{\mathrm{s}} = \frac{\ln\left(\frac{P_{\text{com\_out}}}{P_{\text{com\_in}}}\right)}{\ln\left(\frac{\rho_{\mathrm{s}}}{\rho_{\text{com\_in}}}\right)} \tag{25}$$

where ρ_{s} is the refrigerant density evaluated at inlet entropy and outlet pressure.

For the condenser de-superheating region, while keeping both hot and cold streams unmixed, the energy conservation equation can be expressed as [36]:

$$Q_{\text{csh}} = m_{\text{ref}}(h_{\mathrm{c_1}} - h_{\mathrm{c_2}}) = \mathrm{m_w c_w}(\mathrm{T_{w,out}} - T_{\mathrm{w,c_2}}) = \frac{\left(1 - \mathrm{e}^{-NTU(1-\alpha_{\text{csh}})}\right) C_{\text{csh\_min}}}{1 - \alpha_{\text{csh}} \mathrm{e}^{-NTU(1-\alpha_{\text{csh}})}} (\mathrm{T_{w,out}} - T_{\mathrm{e_2}}) \tag{26}$$

where

$$\alpha_{\text{csh}} = \frac{C_{\text{csh\_min}}}{C_{\text{csh\_max}}} = \frac{\min(\mathrm{m_w}, \mathrm{m_w}\frac{h_{\mathrm{c_1}} - h_{\mathrm{c_2}}}{T_{\mathrm{c_1}} - T_{\mathrm{c_2}}})}{\max(\mathrm{m_w}, \mathrm{m_w}\frac{h_{\mathrm{c_1}} - h_{\mathrm{c_2}}}{T_{\mathrm{c_1}} - T_{\mathrm{c_2}}})} \tag{27}$$

For the condensation region, the energy conservation equation can be expressed as [36]:

$$Q_{\text{cp}} = m_{\text{ref}}(h_{\mathrm{c_2}} - h_{\mathrm{c_3}}) = m_{\mathrm{w}}\, \mathrm{c_w}(\mathrm{T_{w,c_2}} - T_{\mathrm{w,c_3}}) = (1 - \mathrm{e}^{-\mathrm{UA/C}}) m_{\mathrm{w}}\, \mathrm{c_w}(\mathrm{T_{w,c_2}} - T_{\mathrm{c_3}}) \tag{28}$$

For the condenser subcooling region, the energy conservation equation can be

expressed as [36]:

$$Q_{\mathrm{csc}} = m_{\mathrm{ref}}(h_{\mathrm{c_3}} - h_{\mathrm{c_4}}) = \mathrm{m_w c_w}(\mathrm{T_{w,c_3}} - T_{\mathrm{w,c_4}}) = \frac{\left(1-\mathrm{e}^{-NTU(1-\alpha_{\mathrm{csc}})}\right)C_{\mathrm{csc\_min}}}{1-\alpha_{\mathrm{csc}}\mathrm{e}^{-NTU(1-\alpha_{\mathrm{csc}})}}(\mathrm{T_{w,c_3}} - T_{\mathrm{c_4}}) \quad (29)$$

where

$$\alpha_{\mathrm{csc}} = \frac{C_{\mathrm{csc\_min}}}{C_{\mathrm{csc\_max}}} = \frac{\min(\mathrm{m_w}, \mathrm{m_w}\frac{h_{\mathrm{c_3}} - h_{\mathrm{c_4}}}{T_{\mathrm{c_3}} - T_{\mathrm{c_4}}})}{\max(\mathrm{m_w}, \mathrm{m_w}\frac{h_{\mathrm{c_3}} - h_{\mathrm{c_4}}}{T_{\mathrm{c_3}} - T_{\mathrm{c_4}}})} \quad (30)$$

Geometry data for the water-to-refrigerant heat exchanger are shown in Table 1.

Table 1. Parameters of the water-to-refrigerant heat exchanger

Description	Value	Unit
Length	0.355	m
Height	22.9	m
Depth	4.3	℃
Chevron angle	45	◦
Plate thickness	5×10^{-4}	m
Distance between plates	2.1×10^{-4}	m
Enlargement factor	1.17	N/A
Number of plates	500	N/A
Number of water channels	250	N/A

2.2.2 The pump model

Pump power consumption is related to pressure drop and flow rate, which is given as

$$W_{\mathrm{wp}} = \frac{\Delta P m_{\mathrm{f}}}{\eta \rho_{\mathrm{f}}} \quad (31)$$

where W_{wp} is the power of the water pump; η is the efficiency of the water pump which is assumed as 80%, and the efficiency affected by water flow is ignored in this paper; ΔP is the pressure drop in the CDBHE, which includes pressure drop in the inner pipe, in the annular cavity and local pressure drop.

The pressure drop along the pipe can be expressed as:

$$\Delta P = \lambda_{\mathrm{p}} \frac{l_{\mathrm{he}}}{D_{\mathrm{e}}} \frac{v_{\mathrm{f}}^2}{2g} \tag{32}$$

where λ_{p} is the drag coefficient of the pipe; l_{he} is the length of the CDBHE; D_{e} is the equivalent diameter of the pipe; v_{f} is the velocity of the fluid; g is the acceleration of gravity; the λ_{p} of the annular cavity is given as [40]:

$$\lambda_{\mathrm{p,ac}} = \frac{\left(1-D_{\mathrm{ip,out}}/D_{\mathrm{op,in}}\right)^2 \ln\left(D_{\mathrm{ip,out}}/D_{\mathrm{op,in}}\right)}{\left[1+\left(D_{\mathrm{ip,out}}/D_{\mathrm{op,in}}\right)^2\right]\ln\left(D_{\mathrm{ip,out}}/D_{\mathrm{op,in}}\right)+1-\left(D_{\mathrm{ip,out}}/D_{\mathrm{op,in}}\right)^2} \times \frac{64}{\mathrm{Re}} \tag{33}$$

where Re is Reynolds number.

3. Verification of the geothermal sub-model

3.1 Grid independence verification

In order to improve the stability of calculation, it is necessary to test the independence of the grid. The parameters of the virtual CDBHE are shown in Table 2 according to a project being constructed in Tianjin, China.

Table 2. Parameters in the geothermal sub-model

Description	Symbol	Value	Unit
Radius of calculated domain	R	10	m
Borehole depth	Y	2400	m
Ground surface temperature	T_{sur}	12	℃
Geothermal gradient	G	0.025	℃/m
Thermal conductivity of rocks	λ_r	3	W/m·K^{-1}
Heat capacity of rocks	c_{pr}	1040	J/kg·℃$^{-1}$
Design flow rates of circulating water	Q_{w}	30	m^3/h
Inlet temperature	T_{in}	15	℃
Outer diameter of the outer pipe	$D_{\mathrm{op,out}}$	177.8	mm
Inner diameter of the outer pipe	$D_{\mathrm{op,in}}$	168.8	mm
Thermal conductivity of outer pipe	λ_{op}	45	W/m·K^{-1}
Outer diameter of the inner pipe	$D_{\mathrm{ip,out}}$	112.4	mm
Inner diameter of the inner pipe	$D_{\mathrm{ip,in}}$	101.2	mm
Thermal conductivity of outer pipe	λ_{ip}	0.3	W/m·K^{-1}

The uniform grid is utilized in the proposed geothermal sub-model, and the influence of the axial step length (Δy), radial step length (Δr), and discrete time steps

of the underground (Δt_r) and fluid (Δt_f) involved in Eq. (15) - Eq. (18) are shown in Fig. 5. Δr has the greatest impact on the calculation accuracy of the geothermal sub-model, as shown in Fig.5, this is because of that the heat transfer process is most intense in the radial direction. Fig.5(e) indicated that the outlet temperature at the end of the 30th day tends to converge as Δr decreases, and at the same time, the simulation time increases. At the end of the 30th day, when Δr = 0.2m, 0.4m, 0.5m, and 1m, the error is 0.31%, 1.00%, 1.89%, and 6.60%, respectively compared to Δr = 0.1m. Besides, when Δr = 0.1m, 0.2m, 0.4m, and 0.5m, the simulation time cost proportion is 3.07, 2.16, 1.37, and 1.23, respectively compared to Δr = 1m. Accordingly, 0.4m is considered as the step size in the simulation. Besides, Δy, Δt_r, and Δt_f have little influence on the calculation results. Hence, Δy of 10m, Δt_r of 300s, Δt_f of 60s, and Δr of 0.4m are set in the geothermal sub-model finally.

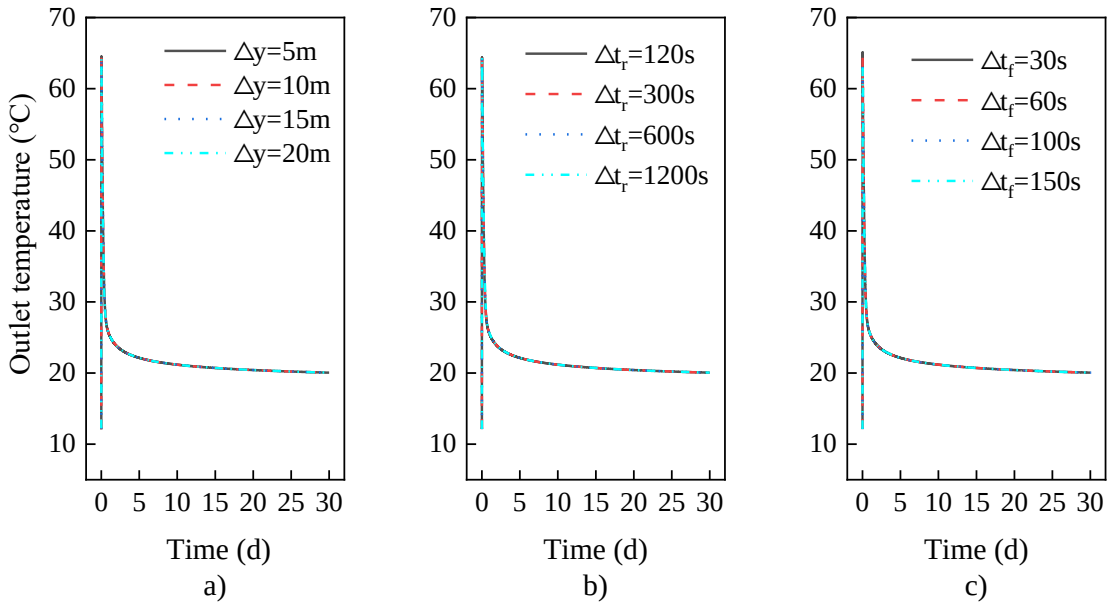

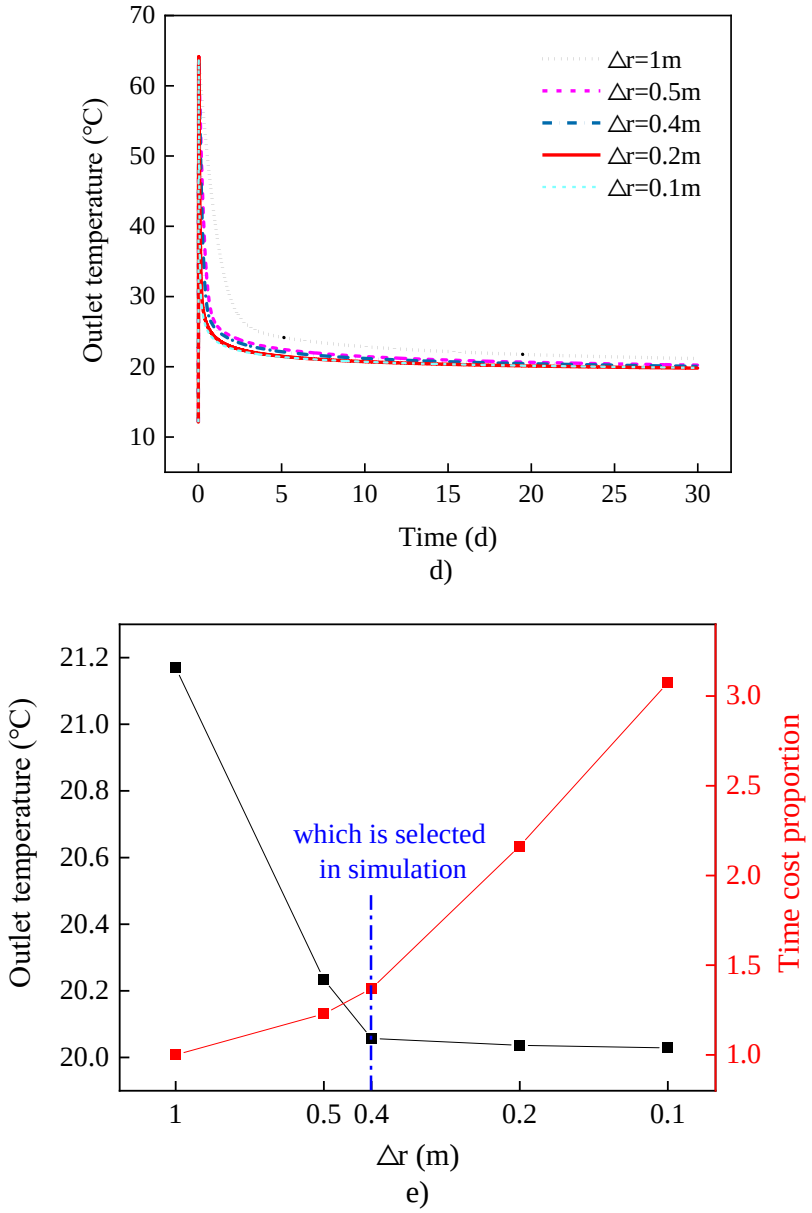

Fig.5 Grid independence tests of the model

3.2 Validation by experimental data

To verify the accuracy of the model, the simulated results were compared with the open test data in Ref. [41]. The geometric and physical parameters of the case are shown in Table 3.

Table 3. Geometric and physical parameters of the case

Description	Symbol	Value	Unit
Borehole depth	*Y*	880	m

Outer diameter of the outer pipe	$D_{op,out}$	17.78	cm
Inner diameter of the outer pipe	$D_{ip,out}$	16.88	cm
Outer diameter of the inner pipe	$D_{op,in}$	8.90	cm
Inner diameter of the inner pipe	$D_{ip,in}$	6.98	cm
Thermal diffusivity of rock-soil	a_e	6.03×10^{-7}	m^2/s
Thermal conductivity of outer pipe	λ_{op}	46.1	$W/m\cdot K^{-1}$
Thermal conductivity of inner pipe	λ_{ip}	0.02	$W/m\cdot K^{-1}$
Ground surface temperature	T_{sur}	30	℃
Design flow rates of circulating water	Q_w	4.8	m^3/h
Geothermal gradient	G	1 (<300m) 13 (≥300m)	K/100m

The power failure has little influence during the test which is shown in Fig. 6. It is clear that the simulated results agree with measured data very well when the operation is stable. The relative error at the end of the 7th day is only 0.86%. And the relative errors within seven days are all less than 10%. The reason for the large error in the initial stage of the operation is that the initial temperature of the water in the model is set to the temperature of the underground rock formations at the same depth which is different from the actual situation. However, the initial temperature only has an influence on the first day of the operation, the error can be ignored when analyzing the operation in a heating season (for 150 days) in this work.

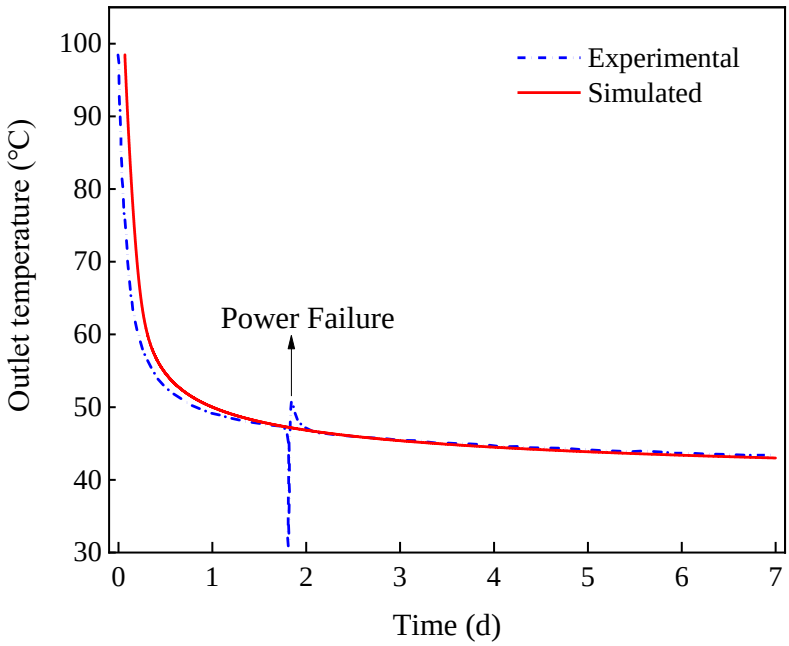

Fig 6. Comparison between simulation results and experiment data

4. Optimization method

Fig. 7 shows the outlet temperature with different flow rates. In Fig. 7, the peak value of the outlet temperature appears within two hours but at different times. The reason for the peak is that the fluid at the bottom of the CDBHE that has a higher temperature at the initial moment reaches the outlet within two hours. However, the later the peak appears as the flow decreases, this is because a small flow rate corresponds to a small flow velocity when the cross section is constant, and it takes a longer time for the fluid to reach the outlet. It is also indicated that the outlet temperature increases as the flow rate decreases in the range of 10 – 45 m^3/h when the operation is stable. After the fluid flows out from the CDBHE, it exchanges heat with the evaporator of the heat pump. A higher outlet (outlet of the CDBHE) temperature means a higher evaporation temperature for the evaporator, which is beneficial to improving the efficiency of the heat pump. In other words, a smaller flow rate is

beneficial to improve the thermal efficiency of the heat pump.

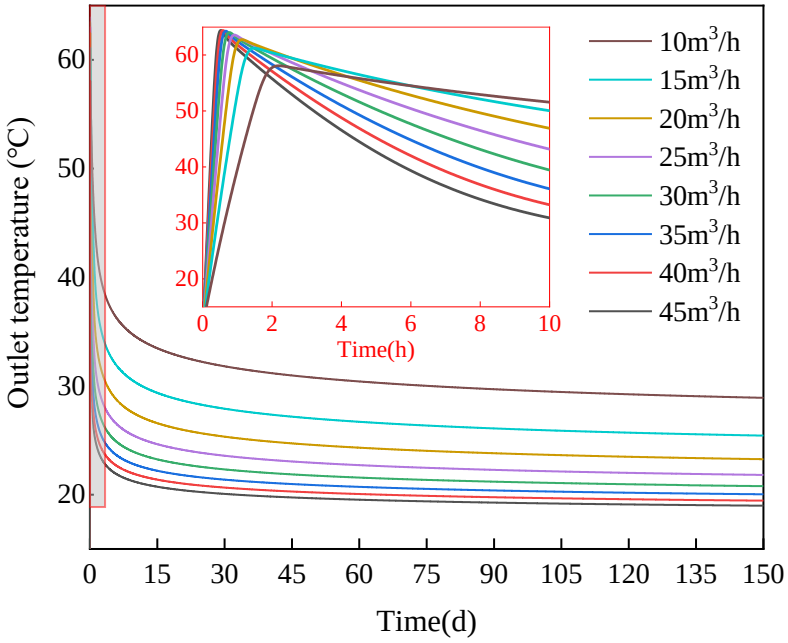

Fig.7 Outlet temperature with flow rate at 30d, 60d, 90d, 120d and 150d

The heat extraction power is given as:

$$P = c_{p,\text{out}} m T_{\text{out}} - c_{p,\text{in}} m T_{\text{in}} \tag{34}$$

Fig. 8 shows the heat extraction power with different flow rates. It is indicated that the heat extraction power increases as the flow rate increases in the range of 10 – 45 m^3/h, and the heat extraction power growth rate slows down when the flow rate is close to 45 m^3/h. It can be inferred from Eq. (19) that the power consumption of the heat pump decreases with the increase of the underground heat extraction power when the heating load is constant. In other words, a larger flow rate is beneficial to reduce the power consumption of the compressor in the heat pump, which is contradictory to the conclusion drawn from Fig. 7. Hence, it is necessary to introduce the heat pump model (Section 2.2.1) to analyze the influence of the flow rate.

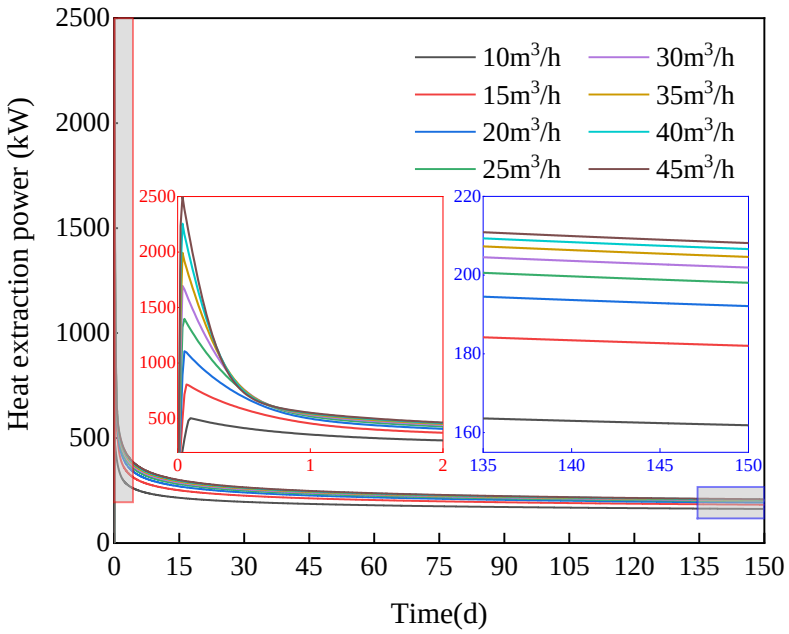

Fig.8 Heat extraction power with different flow rates

The outlet temperature on the first day of operation is around 40°C (as shown in Fig. 7), which is not conducive to the operation of the heat pump. Hence, the fluid and underground temperature distribution after the end of the first day of operation are utilized as the initial conditions of the optimization that lasts for 150 days.

Considering the large difference in heating load between the day (6:00 – 18:00) and night (18:00 – 6:00), two different flow rates are employed every day in the proposed model. Hence, the total power consumption per day is only related to the two flow rates per day (one is set during the day and one is set at night). The relationship between the total power consumption and two flow rates every day can be expressed as:

$$TPC_d = f_d(Q_{d,1}, Q_{d,2}), \quad d = 1, 2, \cdots 150 \tag{35}$$

where TPC_d is the total power consumption on the day d, $1 \le d \le 150$; $Q_{d,1}$ and $Q_{d,2}$ are the two flow rates that are employed on the day d.

The goal of the optimization is to find the minimum of TPC_d for $d = 1, 2, \cdots 150$. Hence, the minimum of TPC_d is a vector with 150 elements which represents the minimum total power consumption every day.

Fig. 9 shows the relationship between the total power consumption and two flow rates on the first day (d =1). It is indicated that $f_d(Q_{d,1},Q_{d,2})$ is a convex function [42], where $Q_{d,1}$ and $Q_{d,2}$ that minimizes the TPC_d are in the range of 10 – 45 m^3/h. For a convex function, it is appropriate to utilize the interior-point method to solve the optimization problem [43]. The optimization problem in this paper can be expressed as:

$$\begin{cases} \min \ f_d(Q_{d,1}, Q_{d,2}), & 1 \le d \le 150 \\ \text{subject to } g_m(Q_{d,1}, Q_{d,2}) \ge 0, & \text{m} = 1,2 \\ g_1 = \min(Q_{d,1} - 10,\ 45 - Q_{d,1}) \\ g_2 = \min(Q_{d,2} - 10,\ 45 - Q_{d,2}) \end{cases} \tag{36}$$

In order to make the optimization process always execute in the feasible region, the penalty function is given as:

$$\varphi_d(Q_{d,1}, Q_{d,2}, r_d) = f_d(Q_{d,1}, Q_{d,2}) - r_d \sum_{m=1}^{2} \ln\left[g_m(Q_{d,1}, Q_{d,2}) \right] \tag{37}$$

where r_d is the penalty factor. According to Eq. (37), the problem is turned into finding $\min \varphi_d$ instead of $\min f_d$. For φ_d, we can input $Q_{d,1}$ and $Q_{d,2}$ that are not limited by the range of 10 – 45 m^3/h, and φ_d can easily be converted to f_d by Eq. (37).

The search path of the optimal flow rates for the operation on the first day is shown in Fig. 9. It is indicated that the approximate optimal rates on the calculated day are 22.58 m^3/h (18:00 – 6:00) and 21.98 m^3/h (6:00 – 18:00), the approximate minimum power consumption is 763.37 kWh.

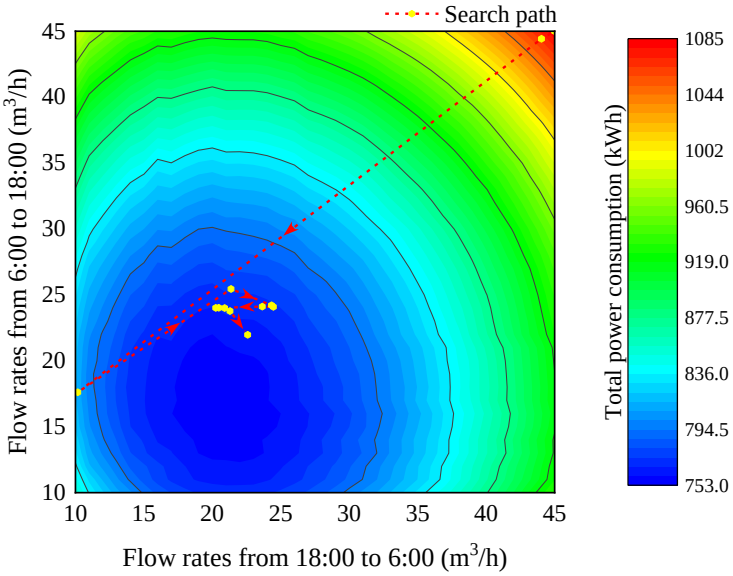

Fig. 9 The relationship between the total power consumption and the flow rates in two periods and the optimization process

The optimization process is carried out day by day during the heating period, following the flow chart depicted in Fig. 10. Among them, the role of ε is to limit the distance of the obtained optimal flow rates and the feasible region. The process of getting the $\min \varphi_d$ is achieved by comparing the gradients of φ_d. Besides, the optimal flow rates on day d-1 are utilized as the starting point of the optimization process on day d ($d = 2 \cdots 150$) to improve the efficiency of the iterative optimization.

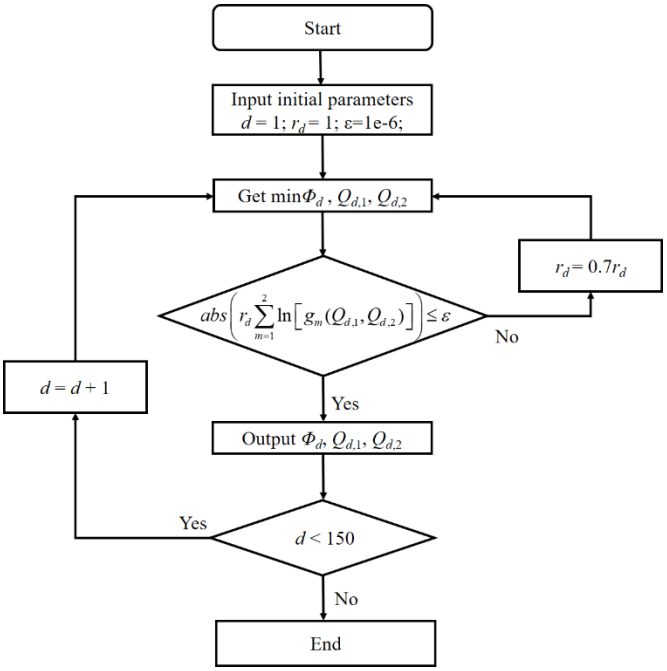

Fig.10 The flow chart of the optimization.

5. Results and discussion

A virtual residential building located in Tianjin (China) with a heat load of 400kW is employed in this work. The temperature of the supply water and the return water for space heating are set to 55℃ and 45℃, and the flow rates of the fluid for space heating are adjusted to adapt to the heat load that varies with the temperature difference between indoor and outdoor. The outdoor temperature of the typical meteorological year in Tianjin is utilized in this work. The indoor temperature is constant at 20℃, and the GSHP system shuts down when the outdoor temperature is higher than 18℃.

Fig.11 shows flow rates of the water in the CDBHE after optimization and indoor and outdoor temperature difference. The two dashed lines are the fitting curves of flow rates and temperature difference respectively. It is indicated that the water flow rate in the CDBHE is constantly changing, not a constant value, and is consistent with the changing trend of the temperature difference between indoor and outdoor over time. Besides, the peak flow rate appears after the peak temperature difference between indoor and outdoor on fitted curves, the reason is that the rate of heat transfer into the underground from the bottom boundary is less than the rate of geothermal heat extraction, when the heat load is near peak. Hence, a larger flow rate is still needed to obtain more heat within a period after the indoor and outdoor temperature difference reaches the peak.

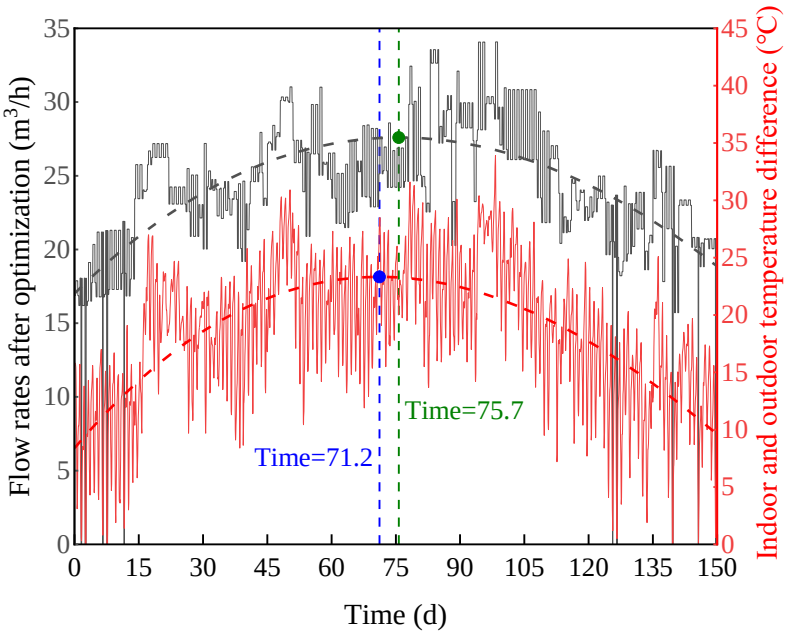

Fig.11 Flow rates after optimization and indoor and outdoor temperature difference

A series of data based on the design flow rate which is 45 m^3/h along the year is utilized as the result of the operation before optimization, compared with the operation data after optimization. Comparing items include:

1) inlet and outlet temperature of the CDBHE
2) heat extraction power from underground
3) power consumption of the heat pump and the water pump as well as the total consumption
4) COP of the heat pump and the TCOP.

Fig.12 shows the changes of inlet and outlet temperature in CDBHE and underground heat extraction power before and after optimization. Fig. 12(a) shows the inlet and outlet temperature of the CDBHE before and after optimization. It is indicated that the outlet temperature increased significantly, but the inlet temperature decreased after optimization. Besides, the fluctuation degrees of inlet temperature is greater than

that of outlet temperature before and after optimization. The reason is that the outlet temperature is mainly affected by the underground heat transfer which is relatively stable, while the inlet temperature (outlet temperature of the evaporator) is mainly affected by the severely fluctuating heat load.

Fig. 12(b) shows the increment of the temperature difference between the inlet and outlet. It is indicated that the temperature difference between the inlet and outlet increases after optimization, and the average increment is 3.17°C, which is 79.43% of that before optimization. The reason is that the amount of heat extraction from the underground does not change much after the optimization (as shown in Fig. 12(c)), and the significantly reduced flow rates in the CDBHE (from 45 to 15-35 m^3/h as shown in Fig. 11) cause a large change in the temperature difference between the inlet and outlet.

Fig. 12(c) shows the difference of heat extraction power after optimization. It is indicated that the heat extraction power decreased during most of the period after optimization. After optimization, the mean value of the difference of heat extraction power is -1.764 kW, which is 0.84% less than the mean heat extraction power before optimization.

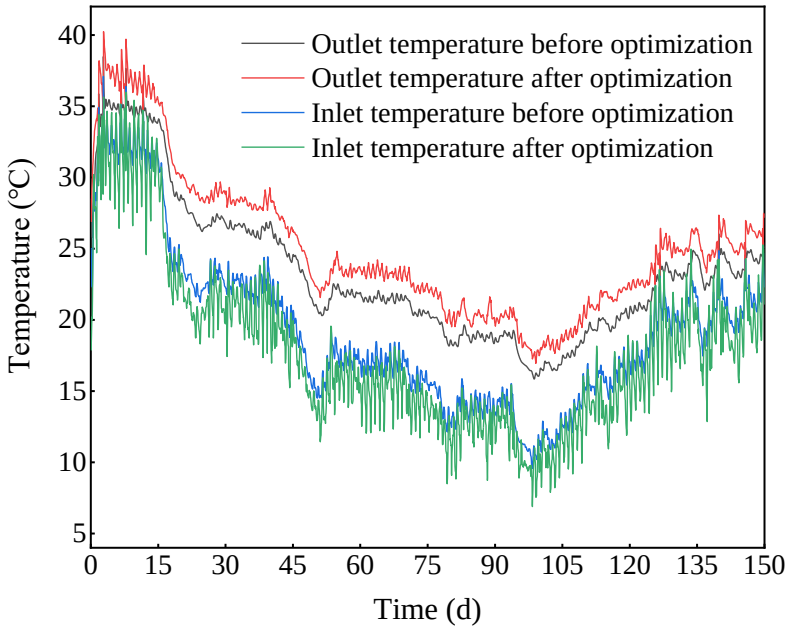
Outlet temperature before optimization
Outlet temperature after optimization
Inlet temperature before optimization
Inlet temperature after optimization
Temperature (℃)
Time (d)

a)

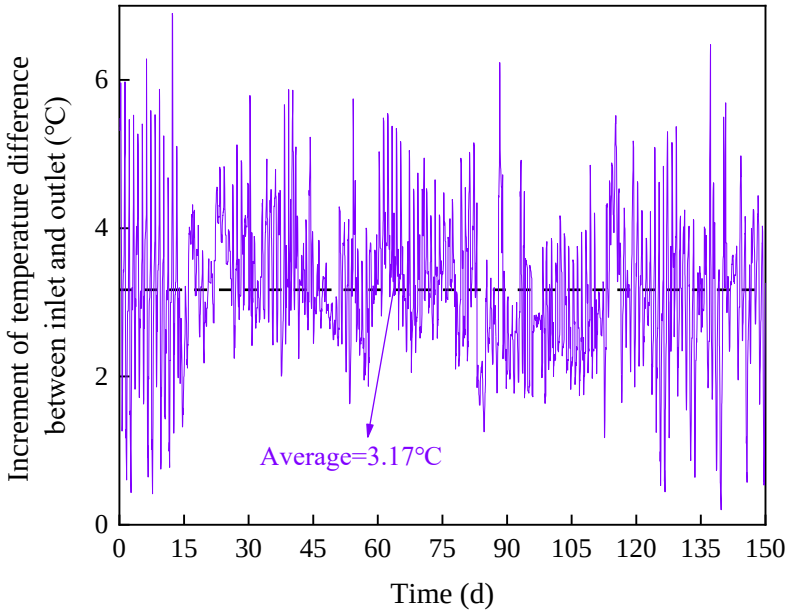
Increment of temperature difference between inlet and outlet (℃)
Average=3.17℃
Time (d)

b)

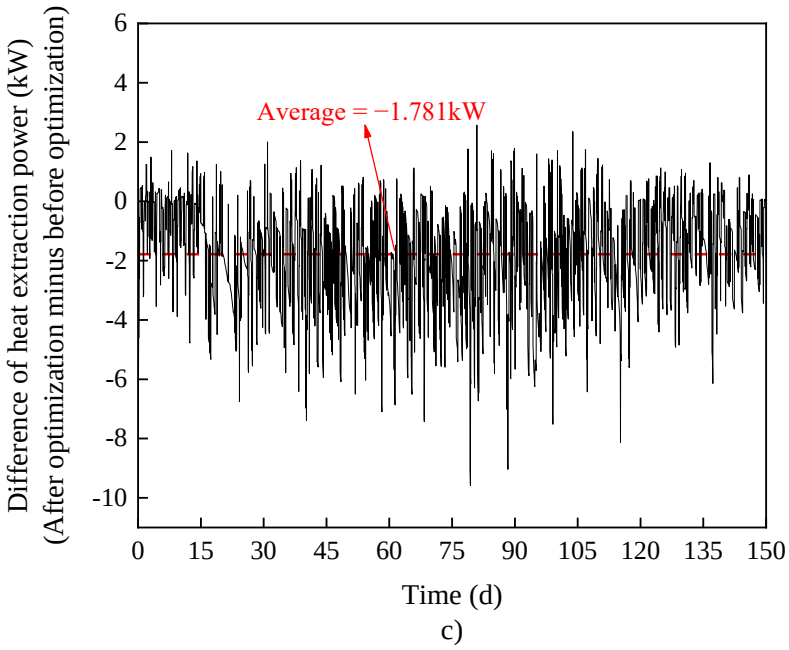

Fig.12 Change of inlet and outlet temperature in CDBHE and underground heat extraction power before and after optimization

Fig. 13 shows the changes of equipment power consumption before and after optimization. It is indicated that the changes in the power consumption of the heat pump are consistent with the changing trend of the indoor and outdoor temperature difference before and after the optimization (Fig. 13(a) and Fig. 13(b)). Fig. 13(c) shows that the heat pump power consumption increased by an average of 2.220kW after optimization. And the power consumption of the water pump has been reduced by an average of 12.885kW, which is 78.45% of that before the optimization.

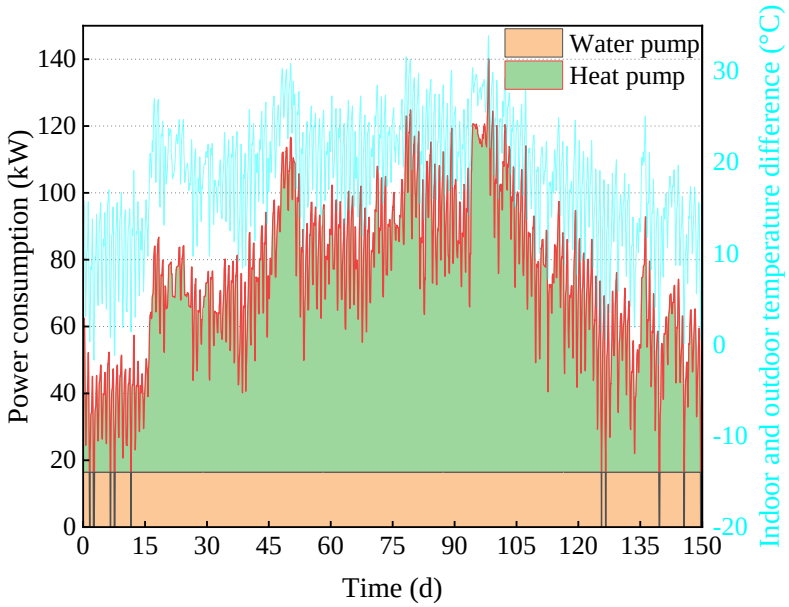

a) Before optimization

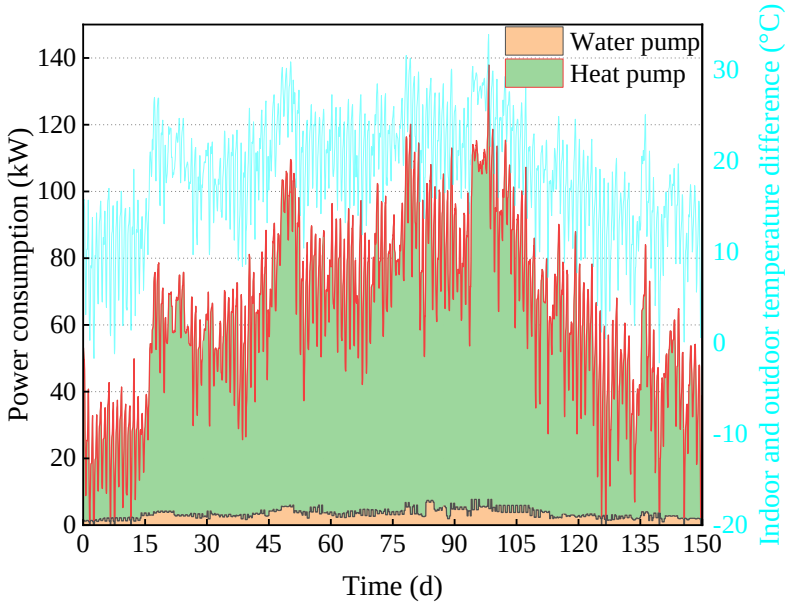

b) After optimization

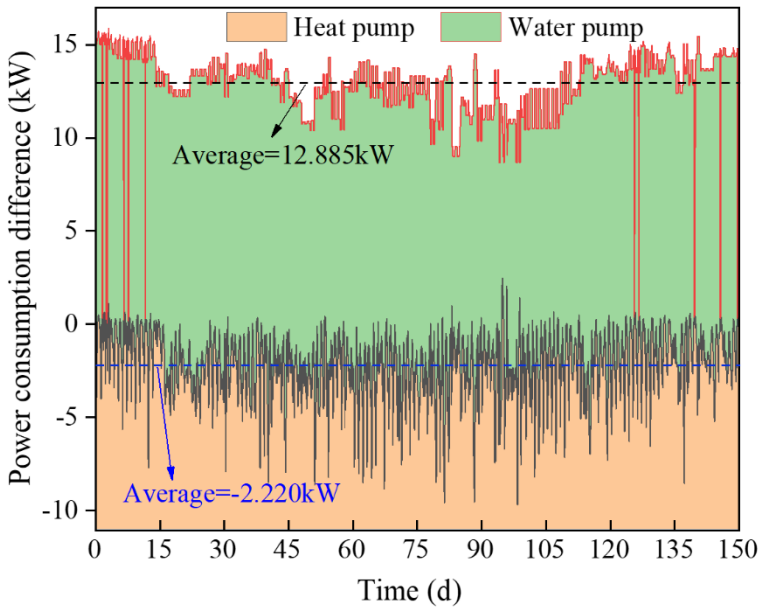

c) Before optimization minus after optimization

Fig.13 Comparison of equipment power consumption before and after optimization

Fig.14 shows the changes of the COP of the heat pump and the TCOP. Fig. 14(a) shows that the COP of the heat pump before and after optimization can be maintained at about 4 in most periods, and can reach 7 in the initial heating stage, reach 5 at the end of heating. The COP is reduced by an average of 0.157 after optimization. Fig. 14(b) shows that the duration when TCOP is lower than 4 accounted for 92.47% of the heating period before optimization, however, the duration when TCOP is higher than 4 accounts for 57.42% of the heating period after optimization. In addition, TCOP increased by 0.783 on average after optimization. And it increases more at the beginning and end of heating when the heat load is relatively small.

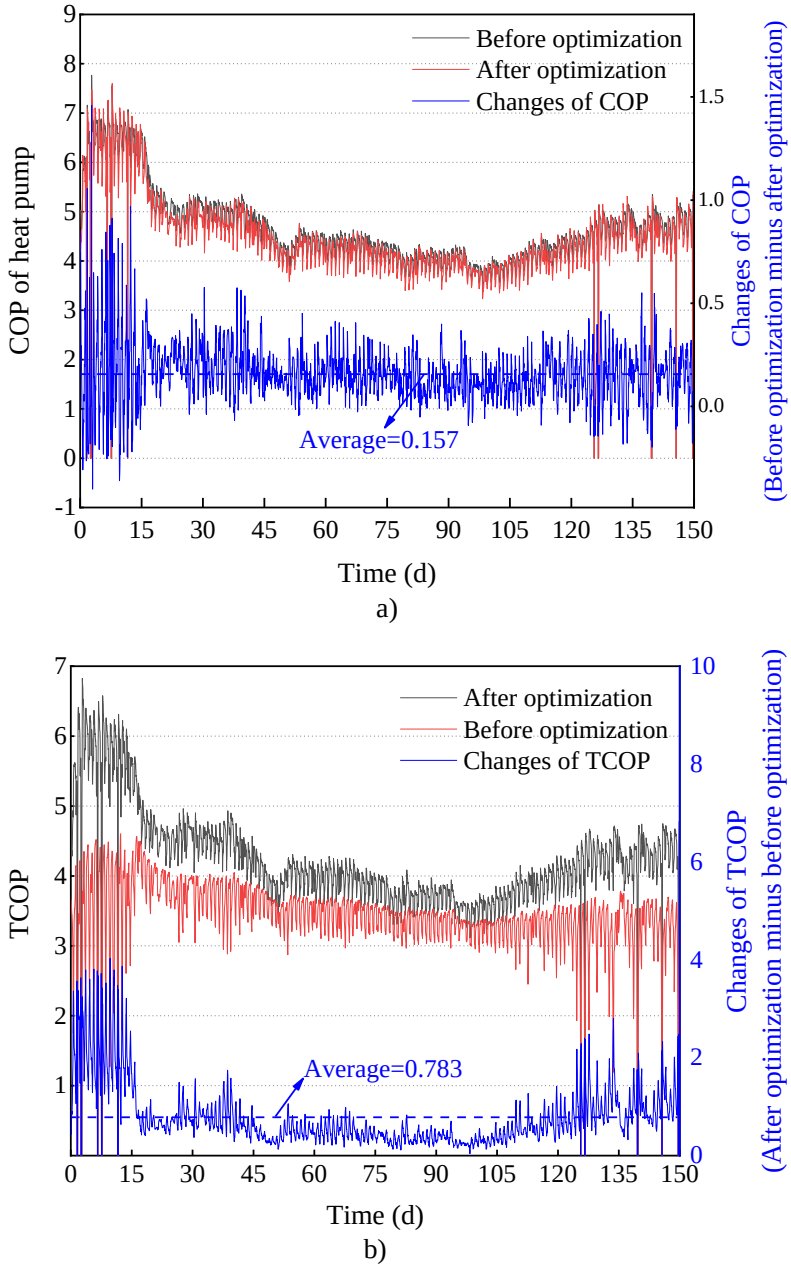

Fig.14 Changes of COP of the heat pump and TCOP

Fig.15 shows the geothermal heat extraction, total power consumption of the heat pump and water pump and their respective power consumption before and after optimization. It is indicated that geothermal heat extraction was reduced by 0.84%, the total power consumption of the heat pump and water pump was reduced by 14.5%, and the heat pump power consumption increased by 3.87%, the power consumption of the water pump was reduced by 79.22% after optimization. Hence, the optimization method

could greatly reduce the power consumption of the water pump under the premise of meeting the heating demand and not increasing the total power consumption of the equipment.

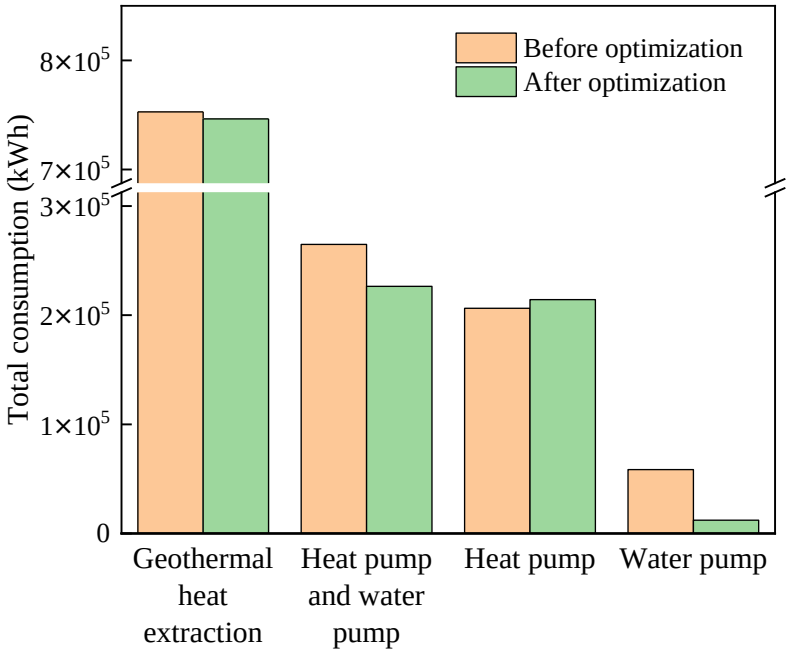

Fig.15 Total consumption before and after optimization

6. Conclusions

An optimization technique based on the interior point method is established in this paper for the operation of the GSHP system that reduces the total power consumption during the heating period significantly. The geothermal sub-model mentioned in the method is verified by data in the literature [41], the proposal of the equipment sub-models refers to the research of Tea Zakula et al [36, 40]. Compared the system operation before and after optimization in a heating period, such as flow rates, geothermal heat extraction power, equipment power consumption, COP, and TCOP, the following conclusions have been drawn:

(1) The change of flow rates after optimization is consistent with the changing trend of the temperature difference between indoor and outdoor over time, and the peak flow

rate appears after the peak temperature difference between indoor and outdoor on fitted curves.

(2) For the CDBHE, the outlet temperature increased and the inlet temperature decreased after optimization, the temperature difference between the inlet and outlet is increased after optimization. However, due to the significant reduction in flow rates after optimization, geothermal heat extraction is reduced.

(3) The power consumption of the water pump is reduced, and the total power consumption of the heat pump and water pump is reduced although the heat pump power consumption is slightly increased after optimization. Besides, TCOP is increased although the COP is reduced after optimization.

(4) For the application of the optimization method, after getting the predicted temperature of the next day, the optimization method proposed for the two flow rates which are set at two time periods respectively every day in the coaxial deep borehole heat exchanger gives appropriate flow rates to match the heating load of the next day.

Increasing the flow rate in the CDBHE is beneficial to increase the heat extraction from underground, but at the same time, it will increase the power consumption of the water pump. The optimization ideas proposed in this paper can reduce the power consumption of the system as much as possible, providing new ideas for the energy-saving operation of the GSHP system.

The optimization is carried out based on the given design parameters of the borehole in this paper. Readers can comprehensively optimize the system design and operation

in combination with the initial investment and income. Besides, limited by the performance of the computer, the minimum power consumption obtained by the method is the sum of the minimum power consumption per day during the heating season. Readers can optimize the flow rates weekly, monthly, or quarterly to get a smaller power consumption.

Acknowledgments

This work was supported by the China National Key R&D Program (Grant No. 2020YFD1100500).

References

[1] Q. Zhu, X. Li, F. Li, D. Zhou, The potential for energy saving and carbon emission reduction in China's regional industrial sectors, Sci Total Environ 716 (2020) 135009.

[2] A. Robert, M. Kummert, Designing net-zero energy buildings for the future climate, not for the past, Building and Environment 55 (2012) 150-158.

[3] X.Q. Zhai, M. Qu, X. Yu, Y. Yang, R.Z. Wang, A review for the applications and integrated approaches of ground-coupled heat pump systems, Renewable and Sustainable Energy Reviews 15(6) (2011) 3133-3140.

[4] Y. Nam, R. Ooka, S. Hwang, Development of a numerical model to predict heat exchange rates for a ground-source heat pump system, Energy and Buildings 40(12) (2008) 2133-2140.

[5] R.A. Beier, S. Morchio, M. Fossa, Thermal response tests on deep boreholes through multiple ground layers, Geothermics 101 (2022) 102371.

[6] W. Mazzotti, J. Acuña, A. Lazzarotto, B. Palm, Deep Boreholes for Ground-Source

Heat Pump, 2018.

[7] J. Acuña, Distributed thermal response tests: New insights on U-pipe and Coaxial heat exchangers in groundwater-filled boreholes, KTH Royal Institute of Technology, 2013.

[8] H. Yin, C. Song, L. Ma, L. Gao, X. Yang, W. Li, J. Zhao, Analysis of flow and thermal breakthrough in leaky downhole coaxial open loop geothermal system, Applied Thermal Engineering 194 (2021) 117098.

[9] I. Sarbu, C. Sebarchievici, General review of ground-source heat pump systems for heating and cooling of buildings, Energy and Buildings 70 (2014) 441-454.

[10] C. Dai, J. Li, Y. Shi, L. Zeng, H. Lei, An experiment on heat extraction from a deep geothermal well using a downhole coaxial open loop design, Applied Energy 252 (2019) 110385.

[11] S. Morchio, M. Fossa, R.A. Beier, Study on the best heat transfer rate in thermal response test experiments with coaxial and U-pipe borehole heat exchangers, Applied Thermal Engineering 200 (2022) 117621.

[12] R.A. Beier, M. Fossa, S. Morchio, Models of thermal response tests on deep coaxial borehole heat exchangers through multiple ground layers, Applied Thermal Engineering 184 (2021) 116241.

[13] H. Holmberg, J. Acuña, E. Næss, O.K. Sønju, Thermal evaluation of coaxial deep borehole heat exchangers, Renewable Energy 97 (2016) 65-76.

[14] P. Li, P. Guan, J. Zheng, B. Dou, H. Tian, X. Duan, H. Liu, Field Test and Numerical Simulation on Heat Transfer Performance of Coaxial Borehole Heat

Exchanger, Energies 13(20) (2020).

[15] Y. Huang, Y. Zhang, Y. Xie, Y. Zhang, X. Gao, J. Ma, Long-term thermal performance analysis of deep coaxial borehole heat exchanger based on field test, Journal of Cleaner Production 278 (2021).

[16] D. Gordon, T. Bolisetti, D.S.K. Ting, S. Reitsma, Short-term fluid temperature variations in either a coaxial or U-tube borehole heat exchanger, Geothermics 67 (2017) 29-39.

[17] D. Gordon, T. Bolisetti, D.S.K. Ting, S. Reitsma, A physical and semi-analytical comparison between coaxial BHE designs considering various piping materials, Energy 141 (2017) 1610-1621.

[18] D. Gordon, T. Bolisetti, D.S.K. Ting, S. Reitsma, Experimental and analytical investigation on pipe sizes for a coaxial borehole heat exchanger, Renewable Energy 115 (2018) 946-953.

[19] L. Fang, N. Diao, Z. Shao, K. Zhu, Z. Fang, A computationally efficient numerical model for heat transfer simulation of deep borehole heat exchangers, Energy and Buildings 167 (2018) 79-88.

[20] S. Morchio, M. Fossa, Thermal modeling of deep borehole heat exchangers for geothermal applications in densely populated urban areas, Thermal Science and Engineering Progress 13 (2019).

[21] J. Liu, F. Wang, W. Cai, Z. Wang, Q. Wei, J. Deng, Numerical study on the effects of design parameters on the heat transfer performance of coaxial deep borehole heat exchanger, International Journal of Energy Research 43(12) (2019) 6337-6352.

[22] X. Song, G. Wang, Y. Shi, R. Li, Z. Xu, R. Zheng, Y. Wang, J. Li, Numerical analysis of heat extraction performance of a deep coaxial borehole heat exchanger geothermal system, Energy 164 (2018) 1298-1310.

[23] K. Jiao, C. Sun, R. Yang, B. Yu, B. Bai, Long-term heat transfer analysis of deep coaxial borehole heat exchangers via an improved analytical model, Applied Thermal Engineering 197 (2021).

[24] P. Hein, O. Kolditz, U.-J. Görke, A. Bucher, H. Shao, A numerical study on the sustainability and efficiency of borehole heat exchanger coupled ground source heat pump systems, Applied Thermal Engineering 100 (2016) 421-433.

[25] X. Zhang, Numerical study of geothermal district heating from a ground heat exchanger coupled with a heat pump system, Applied Thermal Engineering 185 (2021) 116335.

[26] Z. Zhao, Y. Xu, Y.-F. Lin, X. Wang, P. Wang, Probabilistic modeling and reliability-based design optimization of a ground source heat pump system, Applied Thermal Engineering 197 (2021) 117341.

[27] A. Zarrella, G. Emmi, M. De Carli, A simulation-based analysis of variable flow pumping in ground source heat pump systems with different types of borehole heat exchangers: A case study, Energy Conversion and Management 131 (2017) 135-150.

[28] J. Liu, F. Wang, Y. Gao, Y. Zhang, W. Cai, M. Wang, Z. Wang, Influencing factors analysis and operation optimization for the long-term performance of medium-deep borehole heat exchanger coupled ground source heat pump system, Energy and Buildings 226 (2020).

[29] Y. Luo, H. Guo, F. Meggers, L. Zhang, Deep coaxial borehole heat exchanger: Analytical modeling and thermal analysis, Energy 185 (2019) 1298-1313.

[30] X. Hu, J. Banks, Y. Guo, G. Huang, W.V. Liu, Effects of temperature-dependent property variations on the output capacity prediction of a deep coaxial borehole heat exchanger, Renewable Energy 165 (2021) 334-349.

[31] V. Gnielinski, New equations for heat and mass transfer in turbulent pipe and channel flow, Int. Chem. Eng. 16(2) (1976) 359-368.

[32] C. Gao, Y.J.I.c.i.h. Wang, m. transfer, A general formulation of Peaceman and Rachford ADI method for the N-dimensional heat diffusion equation, 23(6) (1996) 845-854.

[33] D.W. Peaceman, J. H. H. Rachford, The Numerical Solution of Parabolic and Elliptic Differential Equations, 3(1) (1955) 28-41.

[34] V.I. Polezhaev, Numerical solution of the system of two-dimensional unsteady Naver-Stokes equations for a compressible gas in a closed region, Fluid Dynamics 2(2) (1967) 70-74.

[35] T.W. Sheu, S. Wang, R. Lin, An implicit scheme for solving the convection–diffusion–reaction equation in two dimensions, Journal of Computational Physics 164(1) (2000) 123-142.

[36] T. Zakula, N.T. Gayeski, P.R. Armstrong, L.K. Norford, Variable-speed heat pump model for a wide range of cooling conditions and loads, Science and Technology for the Built Environment 17(5) (2011) 670-691.

[37] ASHRAE Fundamentals, Handbook, American Society of Heating, Refrigerating

and Air-Conditioning Engineers, 2009.

[38] F.C. McQuiston, J.D. Parker, J.D. Spitler, Heating, ventilating, and air conditioning: analysis and design, John Wiley & Sons2004.

[39] D. Reindl, P.S.A. Klein, A semi-empirical method for representing domestic refrigerator/freezer compressor calorimeter test data, (2000).

[40] Y.H. Kai Xu, Dongyin Wu, The resistance calculation and simulation analysis to annular pipeline, Journal of Changchun Institute of Technology (2015).

[41] K. Morita, W.S. Bollmeier, H. Mizogami, An experiment to prove the concept of the downhole coaxial heat exchanger (DCHE) in Hawaii, (1992).

[42] A.W. Roberts, Convex functions, Handbook of Convex Geometry, Elsevier1993, pp. 1081-1104.

[43] J. Renegar, A mathematical view of interior-point methods in convex optimization, SIAM2001.